Torsional Vibrations of Synchronous Motor Driven Trains Using p-Method

W. J. Chen
Ingersoll-Rand Company,
CENTAC Division,
Mayfield, KY 42066

Synchronous motors produce damaging oscillating torques during startup. If the system is not properly analyzed and designed, the torsional excitation can be very destructive. This paper presents a systematic approach to the dynamic analysis of synchronous motor driven rotating machinery. The p-version of the finite element method is used in the formulation of the equations of motion which provides a great deal of simplicity in the modeling process. The convergence is achieved by increasing the polynomial order of the basis functions of the geometric elements. The system damping matrix can be constructed from the element level or can be calculated by specifying the critical damping factors for a given number of modes of interest. A modified Newmark integration method is employed in the nonlinear transient response calculation. The nonlinearity of the flexible resilient couplings can be easily implemented into this direct numerical integration algorithm. The dynamic stiffness and damping of the resilient couplings are updated at each time step to ensure the dynamic equilibrium. Two examples have been employed to illustrate the validity of the proposed algorithm. The effectiveness, accuracy, and simplicity of the use of p-method on the torsional vibration of synchronous motor driven trains are demonstrated in this paper.

Introduction

Torsional vibration can cause serious failures in rotating geared trains if the system is not properly evaluated and designed. Failures of couplings, keys, shafts, and gear meshes can be experienced in a few startups if they are not adequately designed (Sohre, 1965). In recent years there has been a notable increase in the use of synchronous motors for large compressors due to cost and energy considerations. The use of large synchronous motors and the low level of system damping in the geared trains tend to aggravate the torsional vibration. The motor excitation during startup consists of average and pulsating torques. The magnitudes of the excitation torques vary with speed. For certain types of torque-speed curves, the torsion system can exhibit unstable self-excitation (Shadley et al., 1992). The most serious problem in a synchronous motor driven system is the vibratory torque and stress caused by the motor pulsating torque at twice slip frequency during the startup. The peak-to-peak amplitude of the pulsating torque can be quite large and often exceeds the rated torque. The excitation frequency of the pulsating torque is equal to twice the slip frequency (Brown, 1960). Since the slip frequency varies linearly from line frequency at zero motor speed to zero frequency at synchronous speed, all of the torsional natural frequencies below 120 Hz (60 Hz power system) or below 100 Hz (50 Hz power system) will be excited by the pulsating torque during the startup. Typically, for large compressors with massive motors, several natural frequencies are found to be within the range of excitation frequencies. This requires an accurate prediction of natural frequencies and vibratory torques and stresses during the startup. A comprehensive literature review on the torsional analysis has been presented (Evans et al., 1985). It revealed that only discrete linear mass-elastic models were used in the previous publications and no convergence study was addressed.

Very often, the soft rubber types of nonlinear flexible couplings are used to favorably position the resonant critical speeds and attenuate the torsional vibration in the synchronous motor driven trains. The dynamic stiffness of the coupling changes during the response calculation and it can have a significant effect on the overall response during the resonance. Then step-by-step direct numerical integration method, such as the Newmark Method, has been successfully employed to determine the transient response of linear systems (Szenasi and Nimitz, 1978; Anwar and Colsher, 1979; Evans et al., 1985). The Modal Method has been utilized to reduce the degrees of freedom of the linear system (Jung, 1986). However, the test results have shown that the measured peak responses were considerably lower than the calculated results from the linear theory (Hudson, 1974; Salzman and McComb, 1980). This discrepancy can be attributed to the nonlinearity of the resilient couplings. For a nonlinear system, an iteration scheme, such as Newton-Raphson (Bathe, 1982), is suggested in the numerical integration at each time step to ensure the dynamic equilibrium. The predicted response during and after resonance can have significant error accumulated over the solution steps if the time step is

Contributed by the Technical Committee on Vibration and Sound for publication in the JOURNAL OF VIBRATION AND ACOUSTICS. Manuscript received Feb. 1993; revised Oct. 1993. Associate Technical Editor: J. Mottershead.

large and iteration is not used (Bathe 1982). However, this iteration can become very time consuming if implemented in each time step for the transient response calculation of a synchronous motor startup. In order for the time marching integration to be effective and accurate in the calculation of transient response, an alternative approach is presented in this paper. This approach involves the dynamic stiffness and damping of the nonlinear coupling being updated at each time step and the time step size being decreased in the vicinity of the resonant critical speeds.

During the last few years, there has been considerable research activity in solid mechanics using the p-version of the finite element method (Babuska, 1988). The theoretical basis of the p-method was established and presented in the early 80's (Babuska et al., 1981). The conventional h-version of the finite element method relies upon refining of the mesh of the elements to obtain the convergence. In the p-method, the convergence is achieved by increasing the order of the basis (interpolation) functions within each geometric element. Mesh refinement is therefore not required in the p-method and this feature provides a great deal of simplicity in the design optimization and sensitivity study. The increase of the polynomial order of the interpolation functions employed by the p-method to achieve convergence has been illustrated to be more advantageous than uniform or nearly uniform mesh refinement employed by the h-method (Babuska and Szabo, 1982). The p-method is utilized in this work primarily due to its simplicity of the modeling process and favorable convergence characteristics.

Both steady state and transient torsional analyses are discussed in this paper. The natural frequencies of the system below 120/100 Hz for 60/50 Hz power systems are used in the convergence criterion equation since these frequencies will be excited by the motor pulsating torque during the startup. Once the orders of the polynomials are established in the frequency calculation, the transient analysis can be evaluated by using the same mathematical model. The modified Newmark integration algorithm has been developed and employed in the numerical integration of the nonlinear system equations of motion. A general approach to construct the system damping matrix by specifying damping factors is discussed. Two examples are presented to illustrate the validity of the proposed algorithm. The results are compared with those calculated by using other solution techniques and they appear to be in good agreement.

Equations of Motion

Figure 1 shows a typical three-stage centrifugal compressor driven by a large motor through a rubber coupling, spacer, and a gear coupling. The three high speed stages (pinions) are driven by a bull gear. The system is modeled as an assemblage of shaft elements, concentrated inertias, couplings, gears, etc. Practical considerations should be employed in the modeling of the interference fit connections (Calistrat and Leaseburge, 1972), the effect of shaft penetration (Wilson, 1956), tooth flexibility (Iannuzzelli and Elward, 1984), and the gear backlash (Anwar and Colsher, 1979; Evans et al., 1985). The major components of the rotating assembly are discussed below.

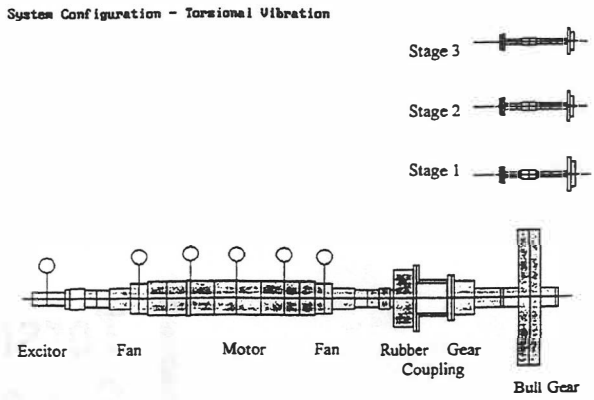

Fig. 1 A typical multi-stage centrifugal compressor

Shaft Element. The p-version of the finite element method is employed in the formulation of the inertia and stiffness matrices of the shaft elements. The pure torsional kinetic energy and strain energy of a uniform element with a circular cross section are given in the following expressions:

$$KE = \frac{1}{2}\int_0^L \rho I_p(\dot{\theta})^2 dx \tag{1}$$

$$PE = \frac{1}{2}\int_0^L GI_p(\theta')^2 dx \tag{2}$$

where $\dot{\theta}$ represents the displacement derivative with respect to time and θ' represents the displacement derivative with respect to the spatial coordinate. The rotational displacement within the element is approximately expressed in the form

$$\theta(\xi,t) = \sum_{i=1}^{p+1} \psi_i(\xi) q_i(t) \tag{3}$$

where the global axial coordinate x is defined from x_k to x_{k+1} and the local coordinate ξ is defined from -1 to 1. The standard element is mapped onto the kth element by

Nomenclature

C = damping
$\mathbf{C}$ = damping matrix
$\underline{\mathbf{C}}$ = modal damping matrix
f_L = line frequency (Hz)
f_s = slip frequency (Hz)
G = shear modulus
I_p = polar moment of inertia
J = inertia
$\mathbf{J}$ = inertia matrix
$\underline{\mathbf{J}}$ = modal inertia matrix
K = stiffness
$\mathbf{K}$ = stiffness matrix
$\underline{\mathbf{K}}$ = modal stiffness matrix
KE = kinetic energy
L = element length
M = dynamic magnifier
N_{cr} = critical speed (rpm)
N_m = motor speed (rpm)
N_{syn} = synchronous speed (rpm)
p = order to Legendre polynomial
P = Legendre polynomial
PE = strain energy
q = generalized displacement
$\mathbf{q}$ = displacement vector
t = time
T = torque
x = global axial coordinate
θ = rotational displacement
ρ = mass density
ξ = local axial coordinate
ψ = basic function
ω = frequency
λ = eigenvalue in state space form
γ = speed ratio
ζ = damping factor
ϕ = eigenvector
φ = eigenvector in state space form
Φ = modal matrix

Subscripts

avg = average
c = coupling
exc = excitation
i,j,k = index
l = linear
m = motor
o = initial
osc = oscillation
r = modal

$$x=\frac{1-\xi}{2}x_k+\frac{1+\xi}{2}x_{k+1} \tag{4}$$

The inverse mapping is

$$\xi=\frac{2x-x_k-x_{k+1}}{x_{k+1}-x_k} \tag{5}$$

The q_i are the coefficients to be determined, and ψ_i are the basis functions. Two types of basis functions proposed by Szabo and Babuska (1991) are utilized in this work:

(1) External (nodal) shape functions

$$\psi_1(\xi)=\frac{1-\xi}{2};\quad \psi_2(\xi)=\frac{1+\xi}{2} \tag{6}$$

(2) Internal shape functions

$$\psi_i(\xi)=\frac{1}{\sqrt{4i-6}}(P_{i-1}(\xi)-P_{i-3}(\xi))\quad i=3,\ 4,\ \ldots\ p+1 \tag{7}$$

where P's are the Legendre's polynomials. These polynomials have very favorable numerical properties and are well suited for computer implementation (Babuska and Szabo, 1982). Substitution of Eq. (3) and into Eqs. (1) and (2), the energy expressions may be written in the form

$$KE=\frac{1}{2}\sum_{i=1}^{p+1}\sum_{j=1}^{p+1}J_{ij}\dot{q}_i\dot{q}_j;\quad \text{where } J_{ij}=\int_{-1}^{1}\rho I_p\psi_i\psi_j d\xi \tag{8}$$

and

$$PE=\frac{1}{2}\sum_{i=1}^{p+1}\sum_{j=1}^{p+1}k_{ij}q_iq_j;\quad \text{where } k_{ij}=\int_{-1}^{1}GI_p\psi_i'\psi_j' d\xi \tag{9}$$

For $p=1$ ($i=1$ to 2), only the external shape functions are included in the formulation and the element will have 2 degrees of freedom (DOF) which is the same as the conventional h-method. The internal shape functions are included only when p is greater than or equal to 2 ($p>=2$). The convergence is achieved by increasing the order of the polynomials within the element rather than refining the mesh. The degree of freedom of the element is equal to the order of the polynomial plus one.

The element inertia and stiffness matrices for a typical element are included in Appendix A for reference. The element material damping properties are not well defined, thus the element damping matrices are difficult to be constructed by the procedures described above. Furthermore, for a geared train system, the damping is mainly due to the couplings, joints, bearings, etc. Therefore, the damping is usually specified at the system level to approximate the overall energy dissipation during the system transient response.

Concentrated Inertia. Concentrated inertias are used to represent the components such as gears, impellers, couplings, etc. From Newton's second law, the equation of motion is given by

$$J\ddot{\theta}=T(\dot{\theta},\theta,t) \tag{10}$$

Coupling. The driven unit is connected to the motor by a coupling or couplings with a spacer. The coupling is the most important component in the elimination of torsional vibration problems, and the coupling is often the only mechanical component that can be changed in the final design stage. Two types of couplings are commonly used in industry which are the gear and rubber type couplings. The gear type couplings are usually modeled as a linear mass-spring system. The rubber type coupling shown in Fig. 2 consists of inner and outer steel members, and separate rubber blocks. The rubber elements provide low stiffness and good damping characteristics compared to the gear type coupling. The disadvantages of the rubber couplings include cost, large weight and moment of inertia, difficult to balance. The rubber type coupling should be modeled as a

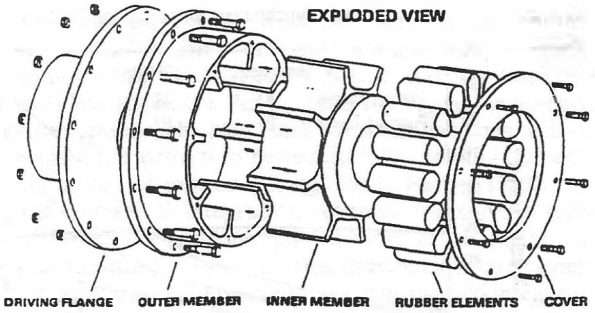

Fig. 2 Flexible coupling exploded view

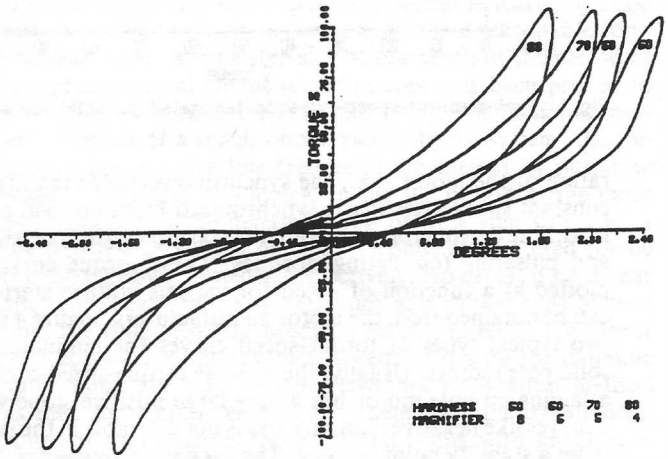

Fig. 3 Flexible coupling hysteresis curves (Holset, 1992)

non-linear component. The nonlinear torque and deflection curves for this type of coupling are available from the manufacturers. Figure 3 shows typical dynamic torque and deflection curves for different rubber grades obtained from a servo-hydraulic torsional test rig (Holset, 1992). It is also known as the hysteresis curve. The nonlinear coupling stiffness characteristics can have a significant effect on the overall response of the system. The coupling damping varies directly with torsional stiffness and inversely with frequency and dynamic magnifier. The dynamic magnifier is dependent upon the hardness of the rubber blocks. Under these conditions the actual torque in the coupling is a function of the instantaneous deflection and velocity across the coupling. The instantaneous torque in the coupling can be determined as follows:

$$T=\frac{\Delta\theta}{|\Delta\theta|}T_s+C_c\Delta\dot{\theta} \tag{11}$$

where T_s is the torque corresponding to a deflection, $\Delta\theta$. The linearlized coupling dynamic stiffness and damping at any instant can be obtained as follows:

$$K_c=\frac{\partial(T_s)}{\partial(\Delta\theta)} \tag{12}$$

$$C_c=\frac{K_c}{M\omega} \tag{13}$$

Where M is the dynamic magnifier of the coupling for a specified rubber hardness.

Motor Torques. Synchronous motors with larger power ratings are gaining in popularity as large compressor drivers for various economic considerations. The synchronous motor starts as an induction motor. When the motor reaches its synchronous speed, a strong, constant magnitude magnetic field is produced in the rotor that locks in step with the stator's rotating magnetic field. The strong interaction between the stator and the rotor magnetic fields causes them to remain locked in step regardless of any changes in the load within the

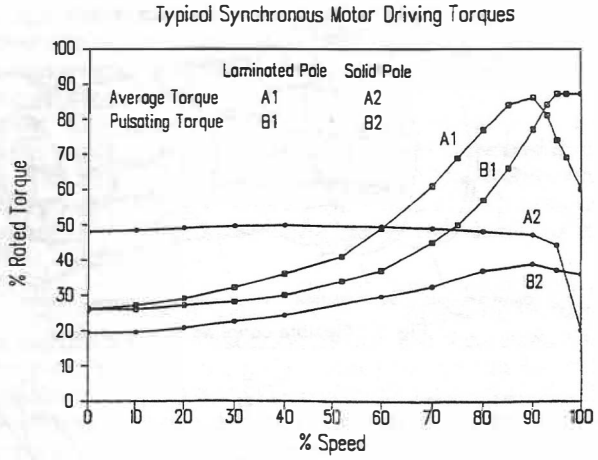

Fig. 4 Typical torque-speed curves for laminated and solid pole motors

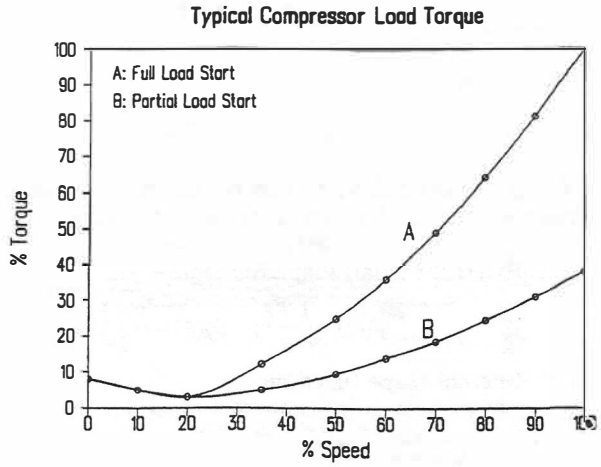

Fig. 5 Typical compressor load torque-speed curves

rating of the motor, i.e., the synchronous motor maintains a constant speed after it has synchronized from no load to full load. The driving torque during the startup consists of average and pulsating (oscillating) torques. These torque curves are plotted as a function of speed for various voltage starts and can be obtained from the motor manufacturers. Figure 4 shows two typical types of torque-speed curves for laminated and solid pole motors. Usually, the average torque-speed curve for a laminated pole motor has a very large positive slope which behaves like negative damping and is not desirable in the system from a stability point of view. The excitation frequency of the pulsating torque is equal to twice the slip frequency and it decreases linearly from twice line frequency at zero motor speed to zero frequency at synchronous speed. The slip frequency, f_s, can be written as

$$f_s = f_L \left(\frac{N_{syn} - N_m}{N_{syn}} \right) \text{ Hz} \tag{14}$$

where f_L is the line frequency (Hz), N_m is the motor speed (rpm) at a given time during the startup, and N_{syn} is the synchronous speed (rpm) calculated by the following expression:

$$N_{syn} = \frac{120 \cdot f_L}{\text{Number of Poles}} \text{ rpm} \tag{15}$$

The motor driving torque at any instant during startup can be expressed in the form (Anwar and Colsher, 1979)

$$T_m = T_{avg} + T_{osc} \sin(\omega_{exc} t) \tag{16}$$

where the excitation frequency, ω_{exc}, is equal to twice the slip frequency

$$\omega_{exc} = 2\pi \cdot 2f_s = 2\pi \cdot 2f_L \cdot \left(\frac{N_{syn} - N_m}{N_{syn}} \right) \text{ rad/sec.} \tag{17}$$

For better numerical integration, the sine component of Eq. (16) is integrated first (Jung, 1986). The motor torque then is expressed in term of angular displacement of the motor.

$$T_m = T_{avg} + T_{osc} \sin(\theta_{exc}) \tag{18}$$

where

$$\theta_{exc}(t) = 2\pi \cdot 2f_L \left((t - \frac{\theta_m}{N_{syn} \cdot 2\pi/60} \right) \tag{19}$$

Load Torques. Figure 5 shows typical compressor load curves for various start conditions. The curves are to be approximately proportional to the square of the speed with a breakaway load at the startup. The load curves for different loading conditions (throttled, full loaded) can be obtained from the compressor manufacturers. Typically, the compressors are partially loaded during the startup.

Assembly. The system equations of motion which describe the behavior of the entire system are obtained by assembling the elemental matrices and vectors. The element coordinates must be transformed to the global coordinate and the displacement continuity must be enforced in the assembly process. For a geared system, the equations of motion of each branch should be referenced to the motor shaft system by multiplying the inertia, damping, and stiffness matrices by γ^2 and multiplying the load vector by γ, where γ is the speed ratio of the branch rotor to the reference rotor.

The assembled system equations of motion are of the form

$$\mathbf{J}\ddot{\mathbf{q}} + \mathbf{C}\dot{\mathbf{q}} + \mathbf{K}\mathbf{q} = \mathbf{T}(\mathbf{q}, t) \tag{20}$$

where $\mathbf{J}$ and $\mathbf{K}$ are real symmetric matrices. Moreover, $\mathbf{J}$ derived from kinetic energy is positive definite and $\mathbf{K}$ derived from potential energy is positive semidefinite. In the case of a nonlinear system, $\mathbf{K}$ could represent the assembly of the element stiffness matrix plus an initial tangent stiffness of the flexible couplings.

In general, the damping matrix $\mathbf{C}$ of a geared train system cannot be constructed from the element level by procedures analogous to the assembly of the element inertia and the stiffness matrices. The torsional critical damping factors for systems with dry type couplings have been reported in the range of 1–5 percent (Mruk et al., 1978; Smalley, 1983; Iannuzzelli and Elward, 1984). Typically, 2 percent of critical damping is used in the transient response calculation for conservative design (Anwar and Colsher, 1979). For systems with resilient rubber couplings, the critical damping of the coupling modes, where the modal displacements are dominated by the coupling, can go up to 6–10 percent.

If the damping matrix in Eq. (20) is specified, the dynamic characteristics of the system are ready to be studied. Otherwise, the damping matrix is calculated from the estimated small percentage of critical damping factors for the modes of interest. Rayleigh damping is determined from two damping factors of two distinguishing modes and the damping in the remaining modes is then determined automatically. A more general approach (Craig, 1981) permits a generalized proportional damping matrix to be generated with specified damping factors for a given number of modes of interest. The procedure is briefly described below.

From the orthogonality relationship, we have

$$\mathbf{\Phi}^T \mathbf{J} \mathbf{\Phi} = \underline{\mathbf{J}} = \text{diag } (J_r) \tag{21}$$

$$\mathbf{\Phi}^T \mathbf{K} \mathbf{\Phi} = \underline{\mathbf{K}} = \text{diag}(K_r) = \text{diag}(\omega_r^2 J_r) \tag{22}$$

$$\mathbf{\Phi}^T \mathbf{C} \mathbf{\Phi} = \underline{\mathbf{C}} = \text{diag}(C_r) = \text{diag}(2\zeta_r \omega_r J_r) \tag{23}$$

where Φ is the modal matrix obtained from the eigenvalue problem

$$(\mathbf{K}-\omega_i^2\mathbf{J})\phi_i=\mathbf{0}, \tag{24}$$

$$\Phi=[\phi_1\phi_2\phi_3\cdots\phi_N] \tag{25}$$

From Eqs. (21), and (23), we have

$$\Phi^{-1}=\underline{\mathbf{J}}^{-1}\Phi^T\underline{\mathbf{J}} \tag{26}$$

$$\mathbf{C}=\Phi^{-T}\underline{\mathbf{C}}\Phi^{-1} \tag{27}$$

Note that $\underline{\mathbf{J}}$ and $\underline{\mathbf{C}}$ are diagonal matrices. Equations (26) and (27) can be combined and expressed in the form

$$\mathbf{C}=\sum_{r=1}^{NDOF}\left(\frac{2\zeta_r\omega_r}{J_r}\right)(\mathbf{J}\phi_r)(\mathbf{J}\phi_r)^T \tag{28}$$

A truncated form of Eq. (28) may be employed to approximate the physical damping matrix for the practical purpose.

Steady State Frequency Analysis

The system undamped and damped natural frequencies can be determined from the following eigenvalue problems, respectively.

$$(\mathbf{K}-\omega_i^2\mathbf{J})\phi_i=\mathbf{0}, \tag{29}$$

for undamped natural frequencies, and

$$\begin{bmatrix}-\mathbf{J}^{-1}\mathbf{C} & -\mathbf{J}^{-1}\mathbf{K}\\ \mathbf{I} & \mathbf{0}\end{bmatrix}\varphi_i=\lambda_i\varphi_i \tag{30}$$

for damped natural frequencies.

Since damping has an imperceptible effect on the torsional natural frequencies of this type of application, the undamped natural frequencies are usually calculated and plotted in the frequency interference diagram (Campbell diagram). The iterative procedure in the p-convergence is terminated at the kth iteration step if the following convergence condition is satisfied:

$$\left(\sum_{i=1}|(\omega_i)_k-(\omega_i)_{k-1}|\right)\le epsilon \tag{31}$$

where $\omega_1, \omega_2, \ldots, \omega_i$ are the natural frequencies of interest and *epsilon* is a small number which defines the desired accuracy. The natural frequencies below twice line frequency were used in this paper. Once the orders of the polynomials are established, the startup transient analysis can be evaluated by using the same mathematical model.

It should be noted that the system stiffness matrix $\mathbf{K}$ is positive semidefinite. The complete geared system is unrestrained and rigid body motion is permitted in the system. For the torsional analysis of a geared train system under study, one (and only one) zero natural frequency will be found in the frequency calculation. The associated mode is referred to as a rigid body mode. The general motion of an unrestrained system consists of a combination of elastic motion and rigid body motion. An eigenvalue shift should be employed for unconstrained vibration problems.

During the transient startup, all of the natural frequencies below twice line frequency will be excited by the pulsating torque. The torsional resonant (critical) speeds during startup are obtained by setting ω_{exc} equal to the natural frequency ω_i. The resonant speeds are expressed as follows:

$$N_{cr}=N_s\cdot\left(1-\frac{\omega_i/2\pi}{2f_L}\right)\quad\text{where } (\omega_i/2\pi)<2f_L,\quad i=1,2,\ldots \tag{32}$$

As the natural frequency decreases, critical speed increases and approaches the synchronous speed. If all the system natural frequencies are above twice line frequency, there will be no resonant speeds during the startup.

Transient Response Calculation

There are several numerical tools and packages readily available for solving a system of first order differential equations. However, excessive computational time and memory storage required in solving the first order differential equations make these tools less attractive. An unconditionally stable numerical integration scheme, the Newmark Method, has been well documented and has proven to be successful in solving the second order equations of motion (Craig, 1981; Bathe, 1982). Typically, the numerical integration schemes for solving second order differential equations require more effort in the computer programming. However, this drawback is overcome by the faster computational time during the numerical integration. The computational time required in the numerical integration is directly proportional to the number of time steps required for the solution. The time step size for the numerical integration must be chosen to obtain accurate results and reasonable computational time. A time step size of one tenth of the period of the highest natural frequency of interest has been proven to be satisfactory (Craig, 1981; Bathe, 1982). For torsional transient response of a synchronous motor driven system, the frequencies below twice line frequency are excited by pulsating torque. Therefore, it is logical to use the period of the twice line frequency in the determination of time step size, i.e., a time step size of 0.0008 or 0.001 seconds can be used for 60 Hz or 50 Hz power systems, respectively. However, if nonlinear components exist in the system, such as a rubber type of coupling, the time step size needs to be decreased as the motor speed approaches the resonant speeds to ensure the dynamic equilibrium. The step-by-step Newmark integration method has been successfully employed to determine the transient response of synchronous motor driven trains with linear couplings (Szenasi and Nimitz, 1978; Anwar and Colsher, 1979; Evans et al., 1985; Jung, 1986). The numerical algorithm for systems with nonlinear resilient couplings is presented below.

The Newmark average acceleration method assumes the acceleration in the time interval t_i to $t_i + \Delta t_i$ to be the average value of the discrete initial and final accelerations:

$$\ddot{q}(t)=\frac{1}{2}(\ddot{q}(t_i)+\ddot{q}(t_i+\Delta t_i)) \tag{33}$$

For simplicity of notation, subscripts i and $i+1$ will be used to represent the time instant t_i and $t_i+\Delta t_i$. Successive integration of Eq. (33) gives the velocity and displacement at time $t_i+\Delta t_i$

$$\dot{q}_{i+1}=\dot{q}_i+\left(\frac{\Delta t_i}{2}\right)(\ddot{q}_i+\ddot{q}_{i+1}) \tag{34}$$

$$q_{i+1}=q_i+(\Delta t_i)\dot{q}_i+\left(\frac{\Delta t_i^2}{4}\right)(\ddot{q}_i+\ddot{q}_{i+1}) \tag{35}$$

Rearranging Eqs. (34) and (35), the velocity and acceleration at time $t_i+\Delta t_i$ are expressed as functions of displacement, velocity, acceleration at time t_i and displacement at time $t_i+\Delta t_i$

$$\dot{q}_{i+1}=\left(\frac{2}{\Delta t_i}\right)(q_{i+1}-q_i)-\dot{q}_i \tag{36}$$

$$\ddot{q}_{i+1}=\left(\frac{4}{\Delta t_i^2}\right)(q_{i+1}-q_i)-\left(\frac{4}{\Delta t_i}\right)\dot{q}_i-\ddot{q}_i \tag{37}$$

The equations of motion are numerically integrated for each time step beginning with the initial conditions of $\mathbf{q}_0=\mathbf{0}$, $\dot{\mathbf{q}}_0=\mathbf{0}$ and all the external torques are suddenly applied. The initial accelerations are obtained from the dynamic equilibrium equation

$$\ddot{\mathbf{q}}_o=\mathbf{J}^{-1}\mathbf{T}_o \tag{38}$$

The equilibrium equations at time $t_i+\Delta t_i$ may be written as follows:

$$\mathbf{J}\ddot{\mathbf{q}}_{i+1}+(\mathbf{C}_1+\mathbf{C}_c)\dot{\mathbf{q}}_{i+1}+(\mathbf{K}_1+\mathbf{K}_c)\mathbf{q}_{i+1}=\mathbf{T}_{i+1}(\mathbf{q}_{i+1},t) \tag{39}$$

where $\mathbf{C}_1$ and $\mathbf{K}_1$ are constant linear damping and stiffness

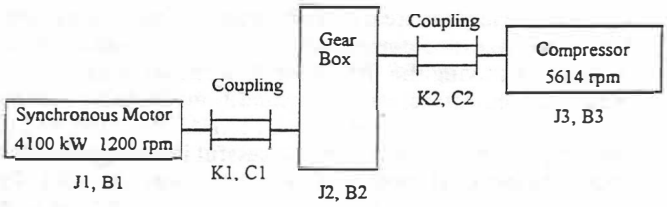

Fig. 6 Three-inertia system model

Table 1 Physical parameters for three-inertia model

Inertia (Kg-m^2)	$J_1 = 473.6$	$J_2 = 554.4$	$J_3 = 1166.2$
Stiffness (N-m/rad)	$K_1 = 8.31E06$	$K_2 = 39.74E06$	
Damping (N-m-sec/rad)	$C_1 = 1882.7$	$C_2 = 4452.8$	
Ground Damping (N-m-sec/rad)	$B_1 = B_2 = B_3 = 2.6$		

All the parameters are referred to the motor shaft

matrices and $\mathbf{C}_c$ and $\mathbf{K}_c$ are the dynamic damping and stiffness of the nonlinear couplings evaluated at the beginning of each time step. $\mathbf{T}_{i+1}$ includes the motor torque, load torque, and coupling torque. Note that the torques added by $\mathbf{C}_c$ and $\mathbf{K}_c$ in the left hand side of the Eq. (39) should also be taken into account in the coupling torque calculation.

Substitution of Eqs. (36) and (37) into Eq. (39) gives NDOF sets of nonlinear equations with NDOF displacements to be determined.

$$\left((\mathbf{K}_1+\mathbf{K}_c)+\frac{2}{\Delta t_i}(\mathbf{C}_1+\mathbf{C}_c)+\frac{4}{\Delta t_i^2}\mathbf{J}\right)\mathbf{q}_{i+1}=\hat{\mathbf{T}}_{i+1}(\mathbf{q}_{i+1},t) \quad (40)$$

and

$$\hat{\mathbf{T}}_{i+1}=\mathbf{T}_{i+1}+\mathbf{J}\left(\frac{4}{\Delta t_i^2}q_i+\frac{4}{\Delta t_i}\dot{\mathbf{q}}_i+\ddot{\mathbf{q}}_i\right)+(\mathbf{C}_1+\mathbf{C}_c)\left(\frac{2}{\Delta t_i}\mathbf{q}_i+\dot{\mathbf{q}}_i\right) \quad (41)$$

A modified Newton-Raphson iteration scheme (Bathe, 1982) can be used to calculate the response from Eq. (40) at each time step. However, this iteration process can be very time consuming if performed in each time step. For the integration algorithm to be effective and accurate in the calculation of transient response, an alternative approach is also presented in this paper. The displacements $\mathbf{q}_{i+1}$ at the right hand side of the Eq. (40) can be approximated in the finite difference form

$$q_{i+1}=q_i+\Delta t_i\dot{q}_i \quad (42)$$

The motor torque, load torque, and coupling torque are projected using the approximate displacements. To ensure the dynamic equilibrium, the time step size needs to be decreased if the system stiffens or the response approaches resonance.

Examples

In order to demonstrate the proposed numerical algorithm, two examples are presented. The first is taken from Vance (1988) and is a three-inertia discrete system consisting of an axial-flow compressor driven by a synchronous motor. No p-convergence is required in this discrete system. This simple system is used to demonstrate the validity of the numerical algorithm. The primary use of this work is for large systems. Thus, a three-stage centrifugal compressor train is also presented to illustrate the ability of the algorithm to deal with more complicated configurations.

Example 1

A schematic and physical parameters for the simple three-inertia system are shown in Fig. 6 and Table 1. The compressor with an inertia of 1166.2 Kg-m^2 was driven by a six-pole 4100 kW synchronous motor through a gear box with a gear ratio of 4.678. Two gear type couplings were used to connect the gear train. The motor synchronous speed calculated by using

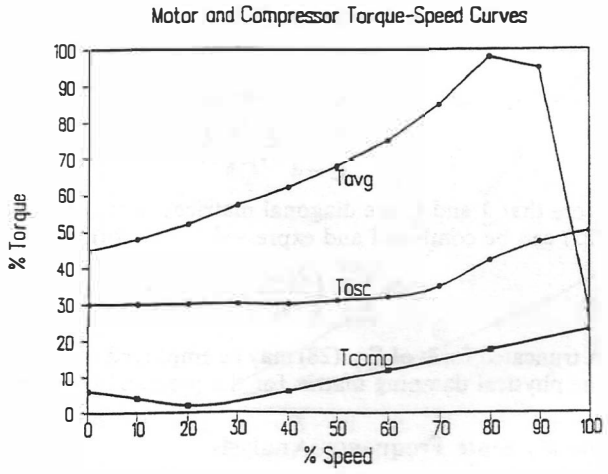

Fig. 7 Torque-speed curves for three-inertia system

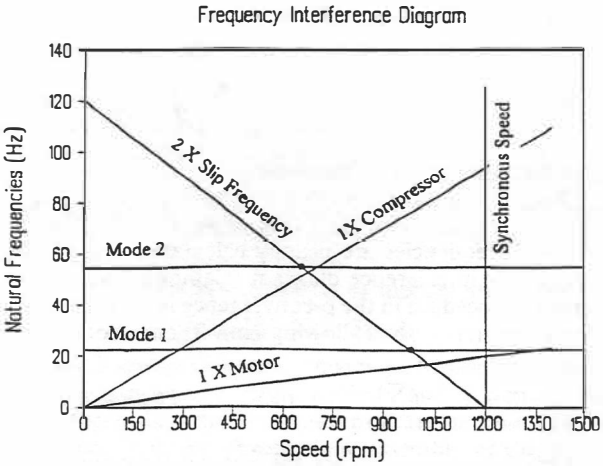

Fig. 8 Frequency interference diagram

Eq. (15) is 1200 rpm, and the compressor has a speed of 5614 rpm. The motor starting torque and compressor load torque curves are shown in Fig. 7. Since the system given is a discrete model, no p-convergence is required in the calculation of system natural frequencies. The two elastic natural frequencies were found to be 22.5 and 54.7 Hz. The resonant speeds excited by the motor pulsating torque during the acceleration are found to be at 653 and 975 rpm. A torsional interference diagram is plotted in Fig. 8. It shows that the system has a good separation margin between critical speeds and operating speed. The logarithmic decrements were found to be 0.0943 and 0.1369 for the first and second modes, respectively. This results in the damping factors of 1.5 percent and 2.2 percent, respectively. Four approaches were used in the transient calculation. A time step size of 0.0008 seconds was used in all of the four approaches for comparison purposes. The numerical integration was performed from 0 to 15 seconds where the motor reached its synchronous speed. First, the linear coupling model was used throughout the integration, the coupling stiffness and damping were not updated at each time step. The dynamic effective stiffness in Eq. (40) was inverted once before the time marching calculation. This is the most effective technique in dealing with systems including linear couplings. Second, the nonlinear coupling model was used (though the equation is linear). The coupling stiffness and damping were updated at each time step to simulate the nonlinear model. Third, the modal damping factors were used to calculate the damping matrix from Eq. (28) instead of using the direct damping coefficients. Fourth, a fifth-order Runge-Kutta method with adap-

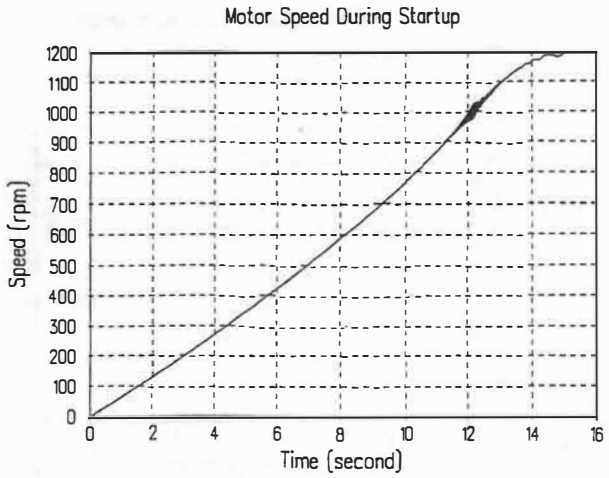

Fig. 9 Motor speed during startup for three-inertia system

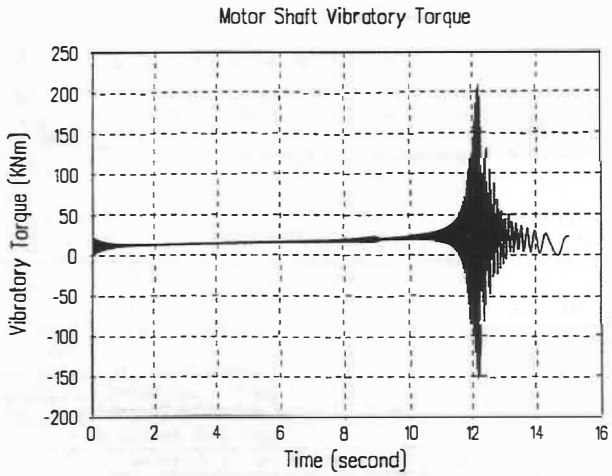

Fig. 10 Motor shaft vibratory torque versus time for three-inertia system

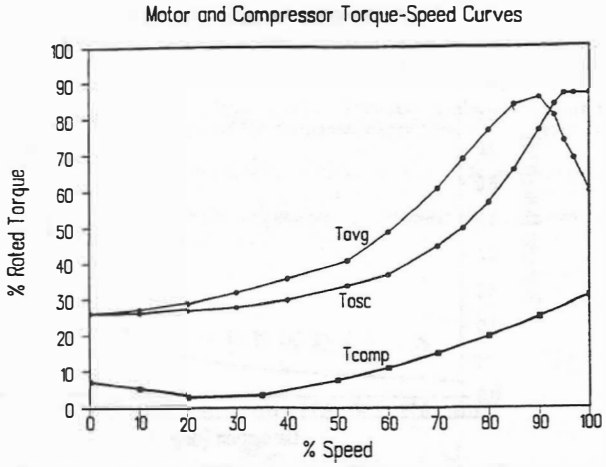

Fig. 11 Motor and compressor torque-speed curves

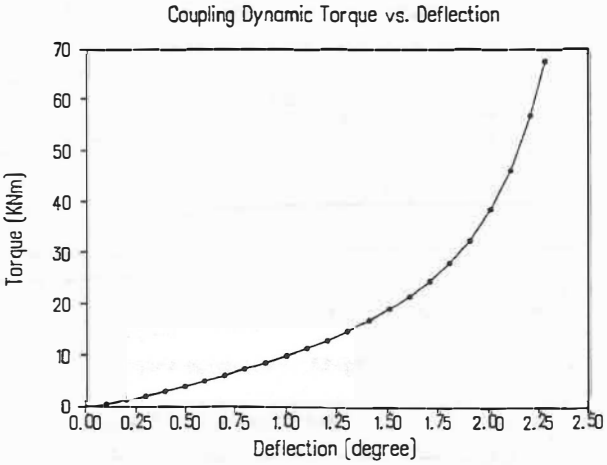

Fig. 12 Coupling dynamic torque versus deflection

tive step size control (Forsythe et al., 1977) was also used in solving the first order differential equation directly as follows:

$$\begin{Bmatrix} \ddot{\mathbf{q}} \\ \dot{\mathbf{q}} \end{Bmatrix} = \begin{Bmatrix} \mathbf{J}^{-1}\mathbf{T} \\ \mathbf{0} \end{Bmatrix} - \begin{bmatrix} \mathbf{J}^{-1}\mathbf{C} & \mathbf{J}^{-1}\mathbf{K} \\ -\mathbf{I} & \mathbf{0} \end{bmatrix} \begin{Bmatrix} \dot{\mathbf{q}} \\ \mathbf{q} \end{Bmatrix} \tag{43}$$

The results from four different approaches are practically identical. The computational time for the transient calculation on a 486DX/50 personal computer were 22, 43, 23, and 118 seconds, respectively. The motor speed versus time during startup is shown in Fig. 9, and the vibratory torque in the motor shaft versus time is shown in Fig. 10. The results are in excellent agreement with the previous publication (Vance, 1988).

Example 2

The second example is a three-stage centrifugal compressor driven by a synchronous motor. A schematic of the system configuration is shown in Fig. 1. A four-pole 2237 kW and 1500 rpm synchronous motor with an inertia of 139 kg-m^2 is the prime driver. The driven compressor which consists of a bull gear shaft and three high speed stages has an equivalent inertia of 224 kg-m^2. A rubber type coupling was installed in the motor side and a gear type coupling was used in the compressor side. The compressor has been operating since 1987 without any mechanical problems. The rubber blocks were inspected recently and appeared to be in good condition.

The torque-speed curves for the motor and compressor are given in Fig. 11. The gear coupling has a linear stiffness of 9.77E07 Nm/rad and the dynamic torque and stiffness of the rubber coupling are shown in Figs. 12 and 13. It shows that the linear approximation is valid only when the coupling deflection is less than 1.0 degree. The nonlinearity gradually increases as the deflection increases up to 1.75 degree. The strength of the nonlinearity increases drastically when the deflection is larger than 1.75 degree.

The finite element model is refined using p-convergence in the frequency calculation. The coupling initial stiffness is much smaller than the adjacent shaft element stiffness, therefore, the convergence was reached in two iterations. The p-version of the finite elements provides a great deal of simplicity in the modeling process though no significant improvement in the accuracy is shown in this example. The first three elastic natural frequencies were found to be 11, 170, and 228 Hz. The mode shape associated with the first elastic mode is plotted in Fig. 14. It shows that the deformation is significant in the flexible coupling.

The startup time is about 11.5 seconds from zero to synchronous speed. A time step size of 0.001 seconds was used in the calculation and it was decreased to 0.0005 seconds when the coupling deflection was greater than 1.0 degree. The motor speed during the transient startup is plotted in Fig. 15 and the coupling vibratory torque is shown in Fig. 16. The maximum coupling vibratory torque was found to be around 32 KNm, and the corresponding deflection is about 1.88 degrees. The system was also analyzed by using Runge-Kutta method (Radomski, 1993). The maximum coupling torque was found to be around 34 KNm with the deflection of 1.91 degrees. This is a good agreement for this large system. To demonstrate the risk involved in using linear approximation, two linear stiff-

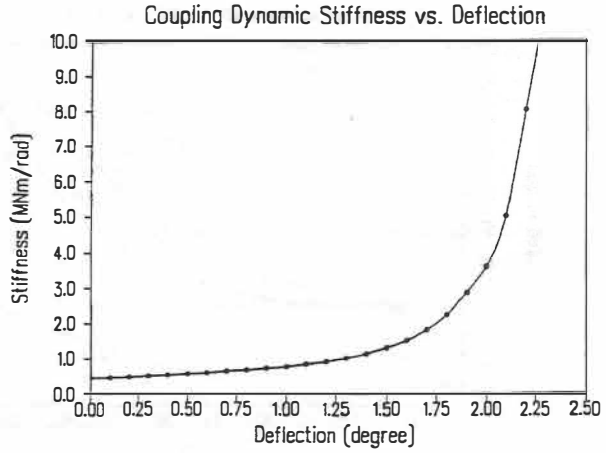

Fig. 13 Coupling dynamic stiffness versus deflection

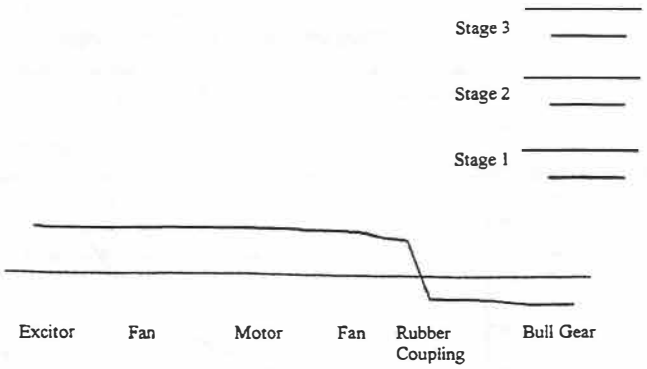

Fig. 14 First mode shape

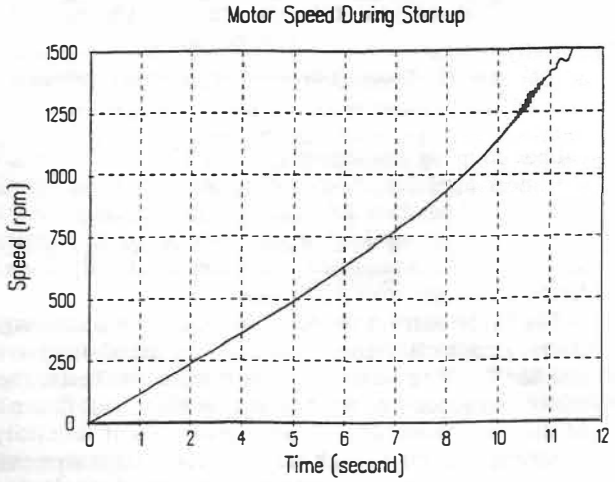

Fig. 15 Motor speed during startup

nesses of 0.470 and 0.987 MNm/rad at initial and applied loads were used in the transient calculation. The calculated coupling deflections were compared with the result obtained from the nonlinear analysis and plotted in Fig. 17. The results show that the linear assumption is invalid in this example. The predicted maximum deflection using the linear assumption is around 5.8 and 2.7 degrees which are not possible without damaging the coupling. The maximum deflection and torque calculated from nonlinear analysis are smaller than those calculated from the linear analysis. Conventional design using linear theory results in shaft diameters that are larger than necessary.

Conclusions

A systematic approach to the dynamic analysis of a synchronous motor driven train has been presented. The p-version of the finite element method has been employed in the formulation of the equations of motion which has provided a great deal of simplicity in the modeling process. A convergence criterion has been established by using the system natural frequencies below twice line frequency. A general approach to construct the system damping matrix by specifying the critical damping factors has been discussed. A modified Newmark integration method has been developed to incorporate the non-

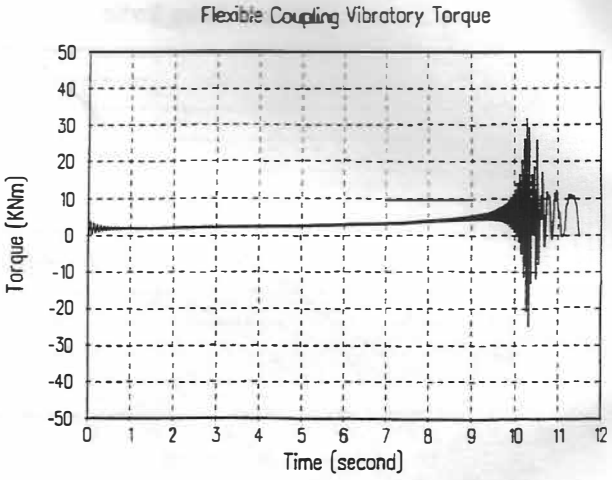

Fig. 16 Coupling torque versus time

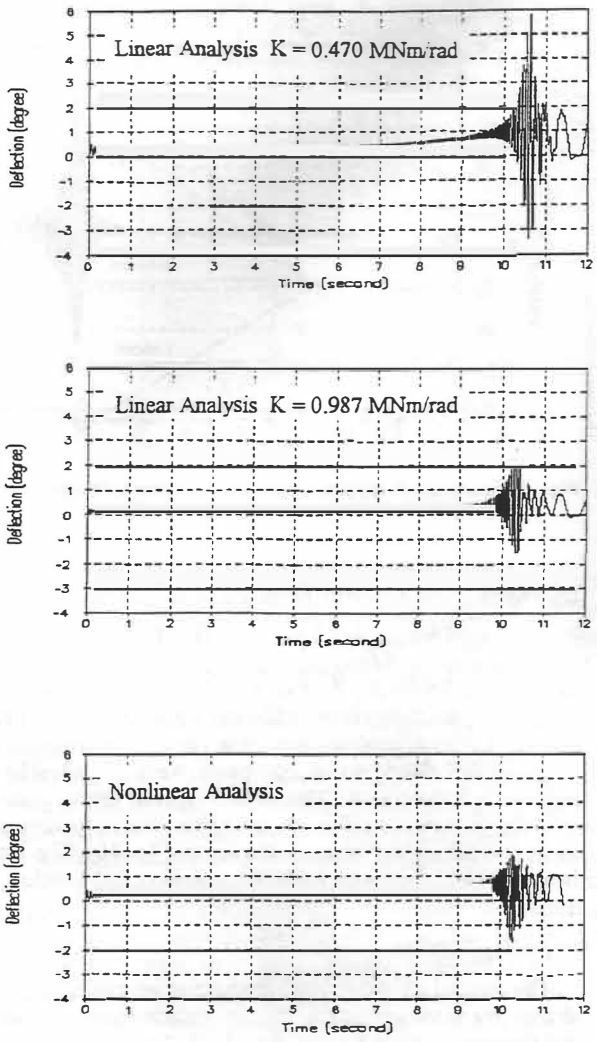

Fig. 17 Comparison of the coupling deflection

linear coupling effect. The proposed algorithm does not require iteration in solving the nonlinear algebraic equation at each time step and the computational time is much less than that of first order differential equation solvers. Two examples have been presented to illustrate the validity of the proposed algorithm. The linear assumption has been shown to be invalid and the nonlinear analysis is required for systems with flexible couplings. The effectiveness and accuracy of the proposed algorithm have been demonstrated in the examples.

Acknowledgments

The author wishes to acknowledge the support and encouragement received from the management of the Ingersoll-Rand Company, Air Compressor Division, in the preparation of this paper and for permission to publish this work. Test data and technical input received from Mr. David Radomski and Mr. Michael Reaney of Holset Engineering Company are gratefully acknowledged.

References

Anwar, I., and Colsher, R., 1979, "Computerized Time Transient Torsional Analysis of Power Trains," ASME Paper 79-DET-74.

Babuska, I., 1988, "The p- and hp- Versions of the Finite Element Method: The state of the Art," *Finite Elements: Theory and Applications*, D. L. Dwoyer, M. Y. Hussaini, and R. G. Voigt, eds., New York, Springer-Verlag.

Babuska, I., and Szabo, B., 1982, "On the Rates of Convergence of the Finite Element Method," *International Journal of Numerical Methods in Engineering*, Vol. 18, pp. 323–341.

Babuska, I., Szabo, B., and Katz, I. N., 1981, "The p-Version of the Finite Element Method," SIAM *Journal of Numerical Analysis*, Vol. 18, pp. 515–545.

Bathe, K. J., 1982, *Finite Element Procedures in Engineering Analysis*. Prentice Hall, NJ.

Brown, R. N., 1960, "A Torsional Vibration Problem as Associated With Synchronous Motor Driven Machines," ASME *Journal of Engineering for Power*, pp. 215–220.

Calistrat, M. M., and Leaseburge, G. G., 1972, "Torsional Stiffness of Interference Fit Connections," ASME Paper 72-PTG-37.

Craig, R. R., 1981, *Structural Dynamics-An Introduction to Computer Methods*, John Wiley & Sons, New York.

Evans, B. F., Smalley, A. J., and Simmons, H. R., 1985, "Startup of Synchronous Motor Drive Trains: The Application of Transient Torsional Analysis to Cumulative Fatigue Assessment," ASME Paper 85-DET-122.

Forsythe, G. E., Malcolm, M. A., and Moler, C. B., 1977, *Computer Methods for Mathematical Computations*, Prentice-Hall, Inc., NJ.

Holset Engineering Co. Ltd, 1992, "Dynamic Response of Holset PM Couplings," England, U.K.

Hudson, J. H., 1974, "Peak Shaft Torques of Three Mass Systems Operating Near or Passing Thru Torsional Resonance," ASME Paper 74-Pet-27.

Iannuzzelli, R. J., and Elward, R. M., 1984, "Torsional/Lateral Coupling in Geared Rotors," ASME Paper 84-GT-71.

Jung, S. Y., 1986, "A Torsional Vibration Analysis of Synchronous Motor Driven Trains by the Modal Method," MS Thesis, Texas A&M University.

Mruk, G., Halloran, J. and Kolodziej, R., 1978, "New Method Predicts Startup Torque," *Hydrocarbon Processing*, April 1987, pp. 181–186.

Radomski, D. J., 1993, "Torsional Transient Analysis of PM40-Synchronous Motor Driven Compressor," Report #1163, Holset Engineering Company.

Salzman, R. W., and McComb, D. S., 1980, "Torsional Vibrations in Synchronous Driven Packaged Centrifugals," *Compressed Air and Gas Institute Technical Digest*, Vol. 13, No. 1.

Shadley, J. R., Wilson, B. L., and Dorney, M. S., 1992, "Unstable Self-Excitation of Torsional Vibration in AC Induction Motor Driven Rotational Systems," ASME *Journal of Vibration and Acoustics*, Vol. 114, April, 1992, pp. 226–231.

Smalley, A. J., 1983, "Torsional System Damping," presented at the 1983 *Vibration Institute 7th Annual Meeting*, Houston, TX.

Sohre, J. S., 1965, "Transient Torsional Criticals of Synchronous Motor Driven, High-Speed Compressor Units," ASME Paper No. 65-FE-22.

Szabo, B. A., and Babuska, I., 1991, *Finite Element Analysis*, John Wiley & Sons, Inc., p. 38.

Szenasi, F. R., and Nimitz, W. W., 1978, "Transient Analysis of Synchronous Motor Trains," *Proceedings of 7th Turbomachinery Symposium*, Texas A&M University.

Vance, J. M., 1988, *Rotordynamics of Turbomachinery*, John Wiley & Sons, Inc., pp. 76–85.

Wilson, W. K., 1956, *Practical Solution of Torsional Vibration Problems*, John Wiley and Sons, Inc.

APPENDIX A

Element Matrices

Element Inertia Matrix

$$J_{11}=J_{22}=\frac{\rho I_p L}{3} \quad J_{12}=J_{21}=\frac{\rho I_p L}{6}$$

For $i>=3$, the non-zero entries are:

$$J_{ii}=\left(\frac{\rho I_p L}{2}\right)\int_{-1}^{1}\psi_i^2 d\xi=\left(\frac{\rho I_p L}{2}\right)\frac{1}{(4i-6)}\int_{-1}^{1}(P_{i-1}(\xi)-P_{i-3}(\xi))^2 d\xi=\left(\frac{\rho I_p L}{2}\right)\frac{2}{(2i-1)(2i-5)}$$

$$J_{i,i+2}=J_{i+2,i}=\left(\frac{\rho I_p L}{2}\right)\int_{-1}^{1}\psi_i(\xi)\psi_{i+2}(\xi)d\xi=-\left(\frac{\rho I_p L}{2}\right)\frac{1}{(2i-1)\sqrt{(2i-3)(2i+1)}}$$

For example, $i=5$, we have

$$\mathbf{J}=\left(\frac{\rho I_p L}{2}\right)\cdot\begin{bmatrix} 2/3 & 1/3 & -1/\sqrt{6} & 1/3\sqrt{10} & 0 \\ & 2/3 & -1/\sqrt{6} & -1/3\sqrt{10} & 0 \\ & & 2/5 & 0 & -1/5\sqrt{21} \\ & \text{Sym.} & & 2/21 & 0 \\ & & & & 2/45 \end{bmatrix}$$

Element Stiffness Matrix

$$k_{11}=k_{22}=\left(\frac{GI_p}{L}\right) \quad k_{12}=k_{21}=-\left(\frac{GI_p}{L}\right)$$

For $i>=3$, the non-zero entries are:

$$k_{i,i}=2\left(\frac{GI_p}{L}\right)$$

For example, $i=5$, we have

$$\mathbf{K}=\left(\frac{GI_p}{L}\right)\begin{bmatrix} 1 & -1 & 0 & 0 & 0 \\ & 1 & 0 & 0 & 0 \\ & & 2 & 0 & 0 \\ & \text{Sym.} & & 2 & 0 \\ & & & & 2 \end{bmatrix}$$